

YOLOO: You Only Learn from Others Once

Lipeng Gu, Mingqiang Wei, *Senior Member, IEEE*, Xuefeng Yan, Dingkun Zhu, Wei Zhao, Haoran Xie, *Senior Member, IEEE*, and Yong-Jin Liu, *Senior Member, IEEE*

Abstract—Multi-modal 3D multi-object tracking (MOT) typically necessitates extensive computational costs of deep neural networks (DNNs) to extract multi-modal representations. In this paper, we propose an intriguing question: May we learn from multiple modalities only during training to avoid multi-modal input in the inference phase? To answer it, we propose YOLOO, a novel multi-modal 3D MOT paradigm: You Only Learn from Others Once. YOLOO empowers the point cloud encoder to learn a unified tri-modal representation (UTR) from point clouds and other modalities, such as images and textual cues, all at once. Leveraging this UTR, YOLOO achieves efficient tracking solely using the point cloud encoder without compromising its performance, fundamentally obviating the need for computationally intensive DNNs. Specifically, YOLOO includes two core components: a unified tri-modal encoder (UTEnc) and a flexible geometric constraint (F-GC) module. UTEnc integrates a point cloud encoder with image and text encoders adapted from pre-trained CLIP. It seamlessly fuses point cloud information with rich visual-textual knowledge from CLIP into the point cloud encoder, yielding highly discriminative UTRs that facilitate the association between trajectories and detections. Additionally, F-GC filters out mismatched associations with similar representations but significant positional discrepancies. It further enhances the robustness of UTRs without requiring any scene-specific tuning, addressing a key limitation of customized geometric constraints (e.g., 3D IoU). Lastly, high-quality 3D trajectories are generated by a traditional data association component. By integrating these advancements into a multi-modal 3D MOT scheme, our YOLOO achieves substantial gains in both robustness and efficiency. Comprehensive experiments on KITTI and Waymo demonstrate the superior performance of our YOLOO over its twenty competitors.

Index Terms—YOLOO, multi-modal 3D MOT, unified tri-modal representation, flexible geometric alignment

I. INTRODUCTION

The growing prevalence of 3D sensors, such as LiDAR and RGB-D camera sensors, has led to the widespread adoption of 3D multi-object tracking (MOT) across diverse domains

L. Gu, M. Wei, W. Zhao are with School of Computer Science and Technology, Nanjing University of Aeronautics and Astronautics, Nanjing, China, and also with Shenzhen Institute of Research, Nanjing University of Aeronautics and Astronautics, Shenzhen, China (e-mail: glp1224@163.com; mingqiang.wei@gmail.com; weizhao0120@nuaa.edu.cn).

X. Yan is with the School of Computer Science and Technology, Nanjing University of Aeronautics and Astronautics, Nanjing, China, and also with the Collaborative Innovation Center of Novel Software Technology and Industrialization, Nanjing, China (e-mail: yxf@nuaa.edu.cn).

D. Zhu is with the School of Computer Science, Jiangsu University of Technology, Changzhou, China (e-mail: zhudingkun@jsut.edu.cn).

H. Xie is with the Division of Artificial Intelligence, School of Data Science, Lingnan University, New Territories, Hong Kong SAR (e-mail: hrxie2@gmail.com).

Y.-J. Liu is with the MOE-Key Laboratory of Pervasive Computing, Department of Computer Science and Technology, Tsinghua University, Beijing, China (email: liuyongjin@tsinghua.edu.cn).

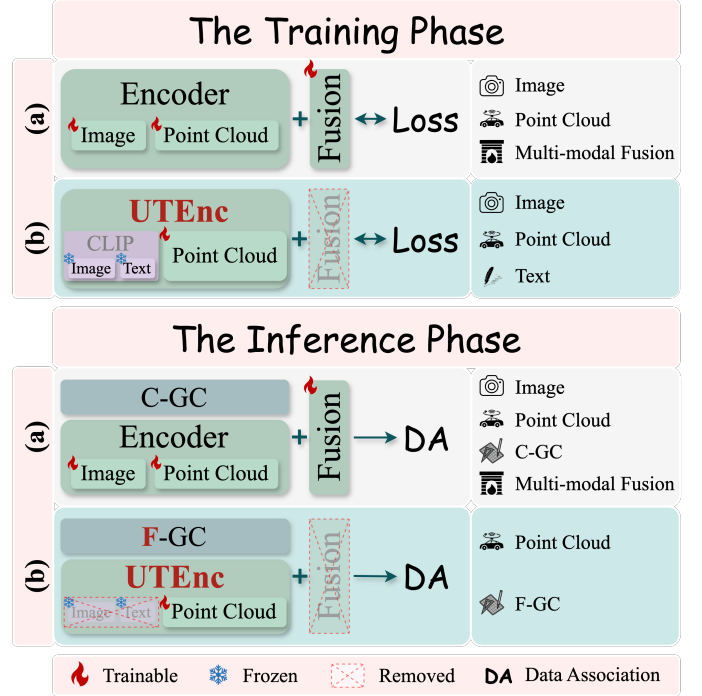


Fig. 1. **Main differences of existing multi-modal methods (a) and YOLOO (b).** (i) *Training Phase*: Unlike prior methods [11]–[14], YOLOO uniquely integrates textual cues and removes a multi-modal fusion module. By jointly learning with image and text encoders from pre-trained CLIP [15], the point cloud encoder within the unified tri-modal encoder (UTEnc) efficiently learns a unified representation from tri-modal data all at once. (ii) *Inference Phase*: YOLOO significantly surpasses prior methods in efficiency by relying solely on the point cloud encoder, whereas others deploy all trained DNN models. (iii) *Geometric Constraint*: Unlike the customized geometric constraint (C-GC) used in prior methods, our flexible geometric constraint (F-GC) enhances the UTR robustness by avoiding the need for scenario-specific fine-tuning.

including autonomous driving, indoor robotics, and unmanned aerial vehicles. Unlike 2D MOT [1]–[6], 3D MOT [7]–[14] leverages 3D spatial information to enhance 3D understanding of the physical environment.

Existing 3D MOT methods primarily fall into two categories: single-modal and multi-modal. The core of both paradigms lies in well-designed constraints that facilitate data association between detections and trajectories, ultimately yielding 3D trajectories.

Single-modal 3D MOT methods [7]–[10] (see Fig. 1 (a)) predominantly rely on customized geometric alignment metrics (C-GAMs), such as BEV Intersection over Union (BEV_IoU) or Centroid Distance (CD), calculated by a customized geometric constraint (C-GC) module. However, to accommodate the varying speeds and sizes of different object categories across diverse scenarios, C-GC must adaptively select more suitable geometric alignment metrics and fine-

tune association thresholds on a per-category and per-scene basis. Despite their effectiveness, these methods still suffer from robustness issues, including frequent identity switches and track fragmentation, particularly in challenging scenarios with crowding, occlusion, or high-speed motion.

To bolster robustness, multi-modal 3D MOT methods [11]–[14] (see Fig. 1 (b)) integrate multi-modal representations from images and point clouds with C-GAMs, effectively mitigating incorrect associations, especially those close in position but distinct in appearance. Nevertheless, acquiring multi-modal representations is computationally demanding, typically involving cross-modal data pre-processing (including alignment, cropping, and resizing), representation encoding using image and text encoders, and multi-modal representation fusion using a fusion module. The complexity of such process, especially in challenging environments (e.g., crowded scenes), has hindered the widespread adoption of multi-modal methods, leading to a predominance of single-modal methods in recent years.

Given the aforementioned challenges of both single- and multi-modal 3D MOT, we pose an intriguing question: *May a modality-specific encoder learn a unified representation encompassing information from both its native modality and other modalities during training?* Through this, multi-modal 3D MOT can be simplified to employ a modality-specific encoder during inference, bypassing pre-processing and encoding of other modalities and multi-modal fusion, fundamentally addressing the issue of low tracking efficiency.

We introduce **YOLOO**, a novel multi-modal 3D MOT solution that redefines the traditional multi-modal paradigm. As shown in Fig. 1 (b), YOLOO concurrently learns from point clouds, images, and text cues during training, without requiring multi-modal fusion. Inference is solely reliant on point cloud data, resulting in efficient and robust performance. Thus, YOLOO attains cross-modal learning capabilities comparable to those exhibited by multi-modal large language models such as ChatGPT-4V and ImageBind [16].

Specifically, YOLOO comprises two core components: a unified tri-modal encoder (UTEnc) and a flexible geometric constraint (F-GC) module. UTEnc integrates point cloud, image, and text encoders, with the latter two adapted from pre-trained visual-language models (VLMs, e.g., CLIP [15]). Our novel unified tri-modal contrastive learning (UTCL) strategy jointly optimizes the point cloud encoder with point cloud data and the rich visual-textual representations extracted from CLIP, while maintaining the parameters of CLIP frozen. This enables the point cloud encoder to learn a unified tri-modal representation (UTR) of point clouds, images, and text cues (describing the object category and spatial location information) all at once, effectively pulling together UTRs of the same object while pushing apart those of different objects. The resulting UTR similarity provides a robust foundation for trajectory-to-detection association. Additionally, to further enhance the UTR robustness, F-GC filters out semantically similar yet geometrically implausible associations while preserving potential candidates. This is accomplished by calculating a flexible geometric alignment metric (F-GAM) that quantifies normalized object distances in the BEV view, independent of specific scene conditions. Lastly, a traditional

data association module integrates the UTR similarity and the F-GAM to accurately associate trajectories with detections across frames, generating high-quality 3D trajectories. With these innovations, YOLOO is a pioneering multi-modal 3D MOT solution that offers both robustness and efficiency.

Why is YOLOO efficient? UTEnc enables the point cloud encoder to learn a UTR from point clouds, images, and text cues during training, while solely relying on the point cloud input at the inference time. This significantly streamlines tracking by eliminating the need for pre-processing and encoding of image and text modalities, and multi-modal fusion. Moreover, F-GC also simplifies the tracking pipeline by obviating the need for scenario-specific fine-tuning.

Why is YOLOO robust? The UTR effectively integrates rich information from point clouds and the comprehensive visual-textual knowledge encoded within pre-trained CLIP, providing robust discriminative cues for accurate trajectory-to-detection association. Moreover, the F-GAM mitigates spurious associations between semantically similar but spatially distant objects, enhancing association reliability.

We conduct a comprehensive evaluation of our YOLOO against twenty competitors on the KITTI and Waymo tracking datasets. Our results consistently demonstrate the superior performance of YOLOO, outperforming all competitors. Our contributions are three-fold:

- We introduce YOLOO, a multi-modal 3D MOT solution that prioritizes the efficiency without sacrificing the robustness. It features UTEnc and F-GC modules.
- UTEnc learns a UTR from point clouds, images, and textual cues in a multi-modal training scheme, yet demands only point cloud data in the inference phase, facilitating efficient and robust 3D MOT.
- F-GC calculates a scene-agnostic F-GAM to discard semantically similar but geometrically implausible trajectory-to-detection associations, further enhancing the UTR robustness.

II. RELATED WORKS

A. 3D Multi-object Tracking

With the advancement of 3D perception technologies (e.g., LiDAR, RGB-D cameras, and multi-view stereo), numerous efforts [7], [8], [14], [17], [18] have been made to advance 3D multi-object tracking (MOT). These methods can be broadly categorized into single-modal and multi-modal types.

1) Single-modal 3D MOT: Single-modal methods (see Fig. 1 (a)), like AB3DMOT [7], CenterPoint [8], and SimpleTrack [19], typically employ customized geometric alignment metrics (C-GAMs) such as BEV Intersection over Union (BEV_IoU) or Centroid Distance (CD) for data association. Despite their simplicity and efficiency, these methods frequently encounter robustness challenges, such as frequent ID switching and interrupted track continuity, especially in crowded environments or during high-speed motion. Moreover, different object categories in various scenarios have distinct moving speeds and sizes, thus necessitating the customization of C-GAMs and association thresholds for each specific category and scene.

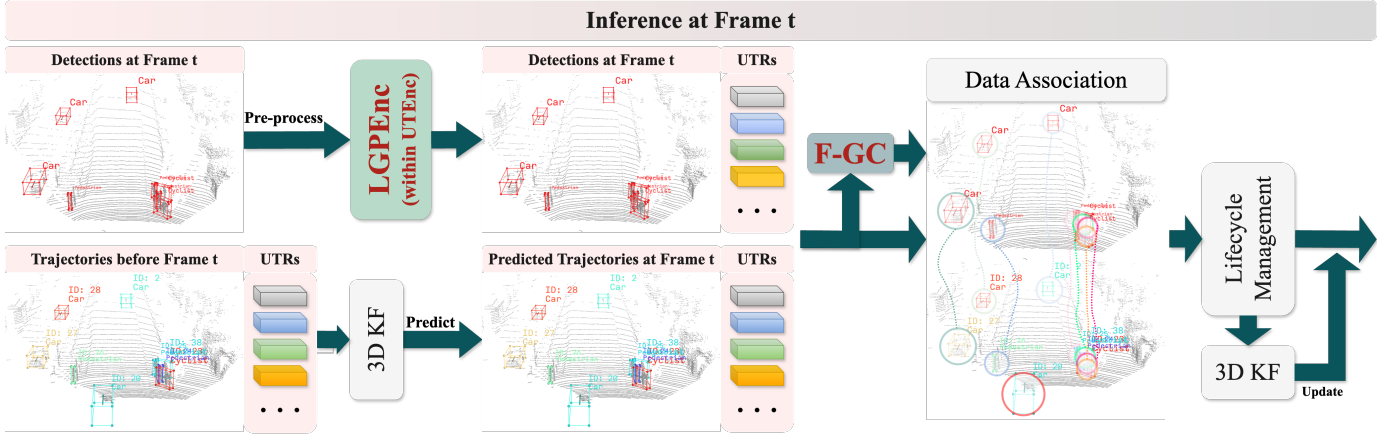


Fig. 2. **Overview of YOLOO.** For simplicity, we only showcase the tracking process between frames $t - 1$ and t . Frame $t - 1$ provides trajectories with corresponding UTRs as input, while frame t offers detections. Detections at frame t undergo pre-processing, including point cloud patch cropping, re-sampling to N points, and feeding into our proposed point cloud encoder (i.e., LGPEnc) within UTEnc to acquire UTRs. Trajectories before frame t are predicted to frame t using a 3D Kalman filter (KF). Then, UTRs from both frames and the flexible geometric alignment metric from F-GC are fed into the data association module to obtain trajectory-to-detection associations. The lifecycle management module handles the birth, death, or association of trajectories, with associated trajectories being updated using the 3D KF. Notably, our lifecycle management and 3D KF modules are consistent with the classic AB3DMOT [7].

2) *Multi-modal 3D MOT*: Multi-modal methods (see Fig. 1 (a)), such as mmMOT [14], JRMOT [11], and FANTrack [13], have been developed to address the previously outlined challenges of insufficient robustness in single-modal methods. By exploiting multi-modal representations extracted from images and point clouds, these methods can effectively disambiguate objects that are spatially close but visually distinct, a limitation of C-GAMs. However, acquiring multi-modal representations is highly time-consuming and labor-intensive, including cross-modal data preprocessing, feature encoding across multiple modalities, and multi-modal feature fusion. This overhead is particularly pronounced in scenes with numerous objects. As a result, recent research has predominantly focused on refining C-GAMs and association thresholds for different scenarios rather than exploring multi-modal representations. This trend raises the question of whether the multi-modal paradigm has become outdated or less competitive in the realm of 3D MOT.

Our YOLOO (see Fig. 1 (b)) redefines the multi-modal paradigm by introducing two novel components: UTEnc and F-GC. UTEnc learns a UTR jointly from point clouds, images, and text prompts during training, while achieving efficient trajectory-to-detection association solely based on point cloud data at inference time. To further enhance the robustness of UTRs, F-GC filters out geometrically implausible associations without requiring scene-specific fine-tuning.

B. Multi-modal Representation Learning

Existing research on multi-modal representation learning has primarily focused on the fusion of two modalities, most commonly image-text and image-point cloud pairs.

1) *Image and Point Cloud*: Image-point cloud-based methods are widely employed in 3D vision tasks, particularly for 3D object detection and tracking. These methods aim to enhance scene comprehension and perception by integrating point cloud representations, rich in spatial geometric information, with image representations, rich in detailed semantic content. For instance, 3D object detection methods like EP-Net++

[20] and PointSee [21] leverage semantically rich images to augment point cloud representations, thereby improving the detection of small and distant objects. Additionally, 3D MOT methods, including mmMOT [14], JMODT [12], FANTrack [13] and JRMOT [11], extract multi-modal representations from both image and point cloud modalities for all objects, then calculate the similarity metric between these representations to establish robust tracking constraints, resulting in more reliable 3D trajectories. However, capturing such representations using complex DNNs becomes increasingly computationally demanding as the number of objects per frame grows, significantly compromising tracking efficiency.

2) *Image and Text*: The advent of pre-trained VLMs, exemplified by CLIP [15] and ChatGPT-4v, has dramatically accelerated the development of image-text-based methodologies. These methods employ image and text encoders to extract embeddings from image-text pairs, aligning them within a unified representation space through contrastive learning. This streamlined architecture facilitates efficient training on large-scale, noisy web datasets, significantly enhancing zero-shot generalization capabilities. Consequently, numerous 2D detection models, such as F-VLM [22], DetPro [23], and OVDet [24], seamlessly achieve open-set detection capabilities by harnessing the zero-shot generalization power of these pre-trained VLMs. Given the inherent cross-modal representation capabilities of each modality encoder within pre-trained VLMs, a compelling question arises: *Can contrastive learning be introduced into multi-modal 3D MOT to allow each modality encoder to learn rich knowledge from both its own and other modalities all at once?* This approach holds the potential to achieve efficient and robust performance using solely a modality-specific encoder, eliminating the necessity for preprocessing, encoding, and fusion of other modalities. However, this avenue remains unexplored.

We propose YOLOO, the first to introduce pre-trained VLMs into 3D MOT for enhancing point cloud encoding. The innovative UTCL strategy injects rich knowledge from image

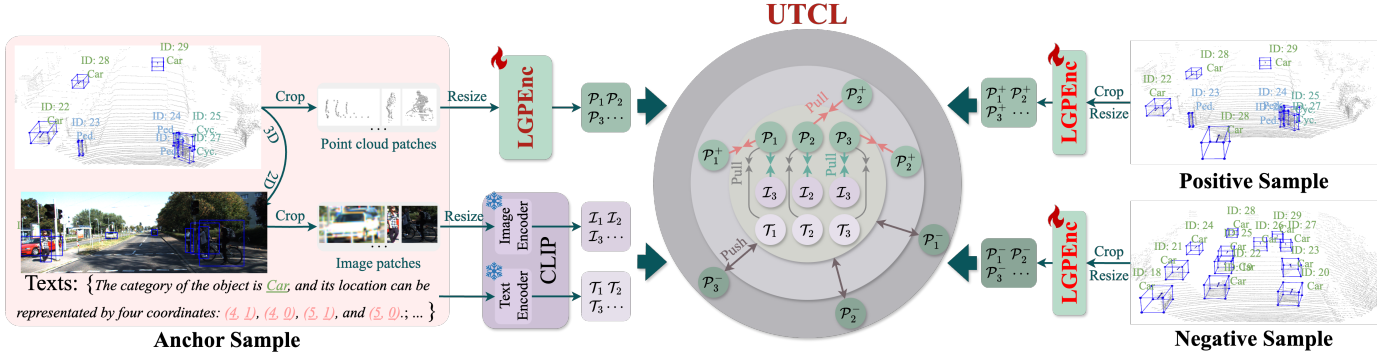


Fig. 3. **Overview of UTEnc.** It integrates image, text, and point cloud encoders, tailored to encode visual objects, text prompts, and spatial point clouds, respectively. Note that the text prompt describes the object's category and positional information on the X-Y plane of the point cloud space. The image and text encoders harness the capabilities of the pre-trained CLIP, whereas the point cloud encoder leverages our innovative local-global point cloud encoder (LGPEnc). During training, the parameters of the image and text encoders are frozen, allowing exclusive focus on training LGPEnc. Through the proposed Unified Tri-modal Contrastive Learning (UTCL) strategy, LGPEnc acquires point cloud information and inherits CLIP's powerful representation capabilities at once. Moreover, LGPEnc develops acute discriminative abilities to differentiate inter-object similarities and differences. As a result, tracking can be efficiently performed using solely LGPEnc, eliminating the need for redundant modules.

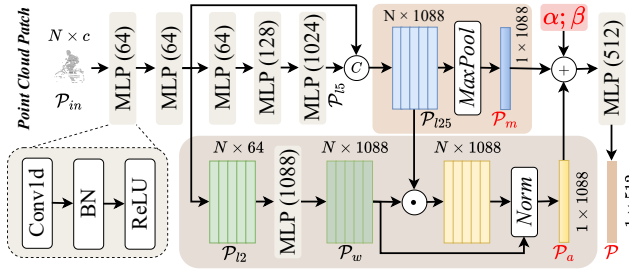


Fig. 4. **Overview of LGPEnc.** It processes a point cloud patch $P_{in} \in \mathbb{R}^{N \times c}$, capturing global $P_m \in \mathbb{R}^{1 \times 1088}$ and local $P_a \in \mathbb{R}^{1 \times 1088}$ features via six MLP layers. These features are subsequently fused using two learnable parameters $\alpha, \beta \in \mathbb{R}^{1 \times 1088}$ and an MLP layer to output the representation $P \in \mathbb{R}^{1 \times 512}$.

and text encoders into the point cloud encoder during training. As a result, the image and text encoders, as well as the multi-modal fusion module, are no longer required at inference time, thus improving the pipeline efficiency.

III. METHOD

A. Overview

To achieve superior performance, current multi-modal 3D MOT methods augment single-modal methods with additional multi-modal representations extracted from images and point clouds through well-designed intricate DNNs. These representations, in conjunction with customized geometric alignment metrics (C-GAMs), serve to establish robust tracking constraints. However, the computational burden introduced by DNN-based feature extraction significantly reduces the efficiency, while the requirement for scene-specific fine-tuning of C-GAM hinders the generalization and increases the overall pipeline complexity. These fundamental limitations necessitate a re-examination of traditional multi-modal 3D MOT to (i) streamline the acquisition of multi-modal representations and (ii) develop more flexible geometric alignment metrics that obviate the need for extensive scene-specific fine-tuning.

We introduce YOLOO, a novel multi-modal 3D MOT solution that redefines the multi-modal paradigm (see Fig. 1

(b) and Fig. 2). YOLOO comprises two core components: a unified tri-modal encoder (UTEnc) and a flexible geometric constraint (F-GC) module. Additionally, conventional data association (DA), 3D Kalman filter (KF), and lifecycle management modules are integrated. Notably, UTEnc integrates a point cloud encoder with image, and text encoders derived from pre-trained CLIP [15]. Through joint training on images, text cues, and point clouds, UTEnc transfers the rich visual-language knowledge from pre-trained CLIP to the point cloud encoder, yielding a unified tri-modal representation (UTR) that facilitates associations between trajectories and detections. This innovation enables efficient multi-modal 3D MOT by solely relying on the point cloud encoder during inference, pioneering the application of pre-trained vision-language models (VLMs) in this domain. Furthermore, F-GC calculates a flexible geometric alignment metric (F-GAM) as a supplementary filter for implausible associations with similar representations but significant positional differences, eliminating the need to fine-tune association thresholds for specific scenarios. Moreover, DA efficiently associates trajectories and detections across frames using the UTR similarity and the F-GAM, generating high-quality 3D trajectories. 3D KF and lifecycle management components are integrated to predict and update 3D trajectory states, and manage their lifecycle, respectively. *These advancements position YOLOO as a formidable contender in the multi-modal 3D MOT domain, owing to its improved tracking efficiency and robust performance.*

Section III-B formally defines the multi-modal 3D MOT problem. Section III-C introduces the proposed UTEnc, followed by a detailed description of F-GC in Section III-D. The DA module is then elaborated upon in Section III-E. Since 3D KF and lifecycle management components are identical to those used in AB3DMOT [7], we omit the details.

B. Problem Formulation

At frame t , input 3D detections are denoted as \mathcal{D}_t . Input 3D trajectories before frame t , denoted as \mathcal{T}_{t-1} , are propagated forward to frame t using the 3D KF, yielding predicted 3D

trajectories $\hat{\mathcal{T}}_t$. First, UTenc subsequently extracts UTRs for all detections. Then, the UTR similarities between \mathcal{D}_t and \mathcal{T}_{t-1} is calculated, forming the cost matrix \mathcal{C}_t^p . Concurrently, F-GC calculates the F-GAM between \mathcal{D}_t and $\hat{\mathcal{T}}_t$, generating the cost matrix \mathcal{C}_t^g as an auxiliary constraint. Leveraging both cost matrices, DA associates detections and trajectories across frames, generating high-quality 3D trajectories \mathcal{T}_t .

C. Unified Tri-modal Encoder

Fig. 1 (a) illustrates that current multi-modal methods [11]–[14] typically utilize sophisticated DNNs, including image and point cloud encoders, as well as a multi-modal fusion module, to extract multi-modal representations from images and point clouds for each object, facilitating robust trajectory-to-detection association. However, the substantial computational cost associated with complex DNNs significantly hampers the efficiency. Moreover, the intricate preprocessing steps involved in aligning and cropping data across different modalities further complicate the overall tracking pipeline. These two factors collectively limit the development of multi-modal paradigms.

To address this, we propose a unified tri-modal encoder (UTenc, see Fig. 3) that is the first to integrate pre-trained CLIP [15] into the 3D MOT domain. UTenc enables the point cloud encoder to learn a unified tri-modal representation (UTR) by jointly learning from point clouds and rich visual-language representations extracted from CLIP. Specifically, UTenc comprises three components: the image encoder for visual objects, the text encoder for text prompts describing the object category and spatial location information, and the point cloud encoder for spatial point clouds. Here, the image and text encoders originate from the pre-trained CLIP, with their parameters frozen during training (see Part III-C1), while the point cloud encoder is our proposed local-global point cloud encoder (LGPEnc, see Part III-C2). Our proposed unified tri-modal contrastive learning (UTCL) strategy (detailed in Section III-C3) aligns point cloud representations with their corresponding image and textual representations into a unified representation space. Meanwhile, UTCL also enhances the discrimination of point cloud representations by maximizing inter-object distances and minimizing intra-object distances.

1) *Image and Text Encoders*: The image encoder processes image patches cropped and resized from each object, while the text encoder handles text prompts describing the object category and its spatial position on the X-Y plane of the point cloud space. The image encoder provides rich semantic information, while the text encoder reinforces category semantics and spatial location guidance. Both encoders produce corresponding representations, denoted as $\mathcal{I} \in \mathbb{R}^{1 \times 512}$ and $\mathcal{T} \in \mathbb{R}^{1 \times 512}$.

2) *LGPEnc*: Advanced point cloud analysis methods, including PointNet++ [25] and Point Transformer [26], exhibit limitations in real-time applications like autonomous driving when processing complex scenes containing numerous objects. To address this, we introduce the local-global point cloud encoder (LGPEnc), illustrated in Fig. 4. LGPEnc efficiently captures intricate point cloud characteristics by integrating local and global features within a streamlined architecture

composed of only seven *MLP* layers and two learnable parameters. Specifically, it processes the point cloud patch of each object, uniformly resamples it to N points, and subsequently generates a representation, formulated as

$$\mathcal{P}_m = \max(\mathcal{P}_{l25}) \in \mathbb{R}^{1 \times 1088}, \quad (1)$$

where $\mathcal{P}_{l25} = \text{concat}(\mathcal{P}_{l2}, \mathcal{P}_{l5}) \in \mathbb{R}^{N \times 1088}$. Here, $\mathcal{P}_{l2} \in \mathbb{R}^{1 \times 64}$ and $\mathcal{P}_{l5} \in \mathbb{R}^{1 \times 1024}$ are features from the second and fifth layers, respectively. The $\max(\cdot)$ and $\text{concat}(\cdot)$ operations denote the maximum pooling and concatenation, respectively. Besides, local features \mathcal{P}_a are derived by applying an attention mechanism to establish interdependencies between feature channels, thereby capturing rich local details, calculated as

$$\mathcal{P}_a = \sum_{i=1}^N \frac{\mathcal{P}_{l25}(i, j) * \mathcal{P}_w(i, j)}{\sum_{j=1}^{1088} \mathcal{P}_w(i, j)} \in \mathbb{R}^{1 \times 1088}, \quad (2)$$

where the attention weights $\mathcal{P}_w \in \mathbb{R}^{N \times 1088}$ are derived from the features \mathcal{P}_{l2} through an *MLP* layer, which quantifies the channel- and point-wise significance of the features \mathcal{P}_{l25} . Subsequently, the global and local features are fused through a weighted sum using learnable parameters $\alpha, \beta \in \mathbb{R}^{1 \times 1088}$. The resulting feature vector is then processed through an *MLP* layer and *L2* normalized to obtain the final point cloud representation, expressed as

$$\mathcal{P} = \text{norm}(\text{mlp}(\alpha * \mathcal{P}_a + \beta * \mathcal{P}_m)) \in \mathbb{R}^{1 \times 512}, \quad (3)$$

where *norm* operation performs the *L2* normalization.

Crucially, leveraging these point cloud representations, the UTR similarity between two objects is formulated as

$$c_{i,j}^p = 1 - \mathcal{P}_i \cdot (\mathcal{P}_j)^T \in [0, 1], \quad (4)$$

where \mathcal{P}_i and \mathcal{P}_j represent point cloud representations of the object in the current and previous frames, respectively.

3) *UTCL*: Through training with cross-modal contrastive learning, pre-trained multi-modal large language models like ImageBind [16] and ChatGPT-4v allow each modality encoder to learn rich knowledge from all other modalities, resulting in semantically rich cross-modal representations. However, existing multi-modal 3D MOT methods [11]–[14] typically employ independent encoders for each modality, where each encoder is restricted to learning knowledge only on its respective single modality. To obtain cross-modal representations, they necessitate fusing representations extracted from disparate encoders. However, this leads to substantial computational overhead attributed to the preprocessing and encoding of multi-modal data and subsequent feature fusion, thereby significantly compromising the efficiency.

To mitigate this inefficiency, we propose the UTCL strategy. By integrating the tri-modal representations into a unified representation space through a cross-modal contrastive loss (\mathcal{L}_{cc}), the point cloud representations are enriched with detailed semantic information derived from images and refined with category-specific semantics and spatial context extracted from text prompts. Additionally, a triplet loss (\mathcal{L}_{tri}) is applied to enhance the discriminative power of point cloud representations in distinguishing object similarities. Thus, the point cloud representation can serve as a unified tri-modal representation

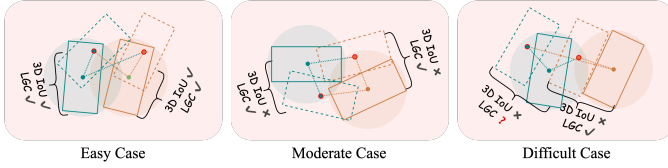


Fig. 5. **Matching is performed using 3D IoU and the F-GAM computed by F-GC.** For visual clarity, all scenarios are presented from a BEV perspective, with objects scaled uniformly. Solid and dashed boxes represent detections and trajectories, respectively. Correct trajectory-to-detection associations are indicated by the same color. These scenarios demonstrate that F-GAM can filter out impossible matches and retain potential candidates with simpler and more flexible computations.

(UTR) of image, point cloud, and text modalities. The UTCL loss is formally defined as

$$\mathcal{L}_{total} = \gamma * (\mathcal{L}_{cc}^{\mathcal{P}, \mathcal{I}} + \mathcal{L}_{cc}^{\mathcal{P}, \mathcal{T}}) + \delta * (\mathcal{L}_{cc}^{\mathcal{P}, \mathcal{P}^+} + \mathcal{L}_{tri}(\mathcal{P}, \mathcal{P}^+, \mathcal{P}^-)), \quad (5)$$

where \mathcal{I} , \mathcal{T} , and \mathcal{P} denote the image, text, and point cloud representations of the anchor object, respectively. \mathcal{P}^+ and \mathcal{P}^- represent point cloud representations of the positive and negative objects, respectively. Positive objects are randomly selected from objects with the same ID within three frames before and after the anchor object. Negative objects are randomly selected from sequences different from the anchor object. The weights γ and δ are assigned to the losses \mathcal{L}_{cc} and \mathcal{L}_{tri} , respectively. The loss \mathcal{L}_{cc} is formulated as

$$\mathcal{L}_{cc}^{\mathcal{P}, F} = \sum_{i,j \in \mathcal{B}} -\frac{1}{2} \log \frac{\exp\left(\frac{\mathcal{P}_i F_j}{\tau}\right)}{\sum_k \exp\left(\frac{\mathcal{P}_i F_k}{\tau}\right)} - \frac{1}{2} \log \frac{\exp\left(\frac{\mathcal{P}_i F_j}{\tau}\right)}{\sum_k \exp\left(\frac{\mathcal{P}_k F_j}{\tau}\right)}, \quad (6)$$

where $F \in \{\mathcal{I}, \mathcal{T}, \mathcal{P}^+\}$. \mathcal{B} signifies the batch size, and τ is a learnable temperature parameter. Besides, the other loss \mathcal{L}_{tri} is formulated as

$$\mathcal{L}_{tri}(\mathcal{P}, \mathcal{P}^+, \mathcal{P}^-) = \frac{1}{\mathcal{B}} \sum_{i \in \mathcal{B}} \max \left(\max_{k \in \mathcal{B}} \|\mathcal{P}_i - \mathcal{P}_k^+\| - \min_{k \in \mathcal{B}} \|\mathcal{P}_i - \mathcal{P}_k^-\| + \epsilon, 0 \right), \quad (7)$$

where $\|\cdot\|$ denotes the cosine distance between two embeddings. ϵ represents the margin.

D. Flexible Geometric Constraint

While UTR demonstrates strong discriminative power, it remains susceptible to erroneous trajectory-to-object associations when representations are similar but geometric locations diverge significantly. To address this, conventional methods [7], [17]–[19] typically employ a customized geometric constraint (C-GC) module to quantify object-level geometric distances using customized geometric alignment metrics (C-GAMs). However, due to the varying speeds and scales of objects across different scenes, C-GC necessitates

careful design of C-GAMs and empirical tuning of association thresholds for each scenario. This heuristic-driven approach exhibits limited adaptability to new scenarios and is prone to failure in challenging conditions (refer to moderate and difficult cases in Fig. 5).

To address this limitation, we introduce a flexible geometric constraint (F-GC) module to compute a category and scene-invariant flexible geometric alignment metric (F-GAM), which is defined as

$$c_{i,j}^g = \frac{\|(x_i - x_j, y_i - y_j)\|}{\min(\|(l_i, w_i)\|, \|(l_j, w_j)\|)}, \quad (8)$$

where $\|\cdot\|$ denotes the Euclidean distance. (x_i, y_i) and (l_i, w_i) represent the center and dimensions (length and width) of the detection $\mathbf{d}_i \in \mathcal{D}_t$ in the BEV perspective. Similarly, (x_j, y_j) and (l_j, w_j) represent the predicted trajectory $\mathbf{t}_j \in \mathcal{T}_t$. Objects are considered incompatible if c^g exceeds 1; otherwise, they are potential matches.

To vividly illustrate the advantages of F-GC, Fig. 5 presents three representative scenarios. In the easy scenario, both 3D IoU and F-GAM accurately match detections and trajectories. However, the moderate scenario reveals the limitations of 3D IoU, as it associates detections with incorrect trajectories due to their high 3D IoU values. In contrast, F-GAM correctly identifies the correct associations. In the difficult scenario, 3D IoU mistakenly discards correct associations due to zero 3D IoU values, while F-GAM retains potential associations for further evaluation with UTR. The flexibility of F-GAM stems from its independence from custom geometric constraints and strict association thresholds. Coupled with its simple computations, F-GAM can effectively eliminate implausible matches while preserving a broader range of potential candidate trajectories for subsequent consideration with UTR.

E. Data Association

Like existing methods [7], [13], [14], [17], [27], our DA module is straightforward, using well-designed constraints to associate trajectories and detections between adjacent frames. Specifically, our constraints are the UTR similarity (see Eq. 4) and the LGA metric (see Eq. 8). The cost matrix between adjacent frames is calculated as

$$\mathcal{C} = \begin{bmatrix} c_{1,1}^p + c_{1,1}^g & \cdots & c_{1,N_t}^p + c_{1,N_t}^g \\ c_{2,1}^p + c_{2,1}^g & \cdots & c_{2,N_t}^p + c_{2,N_t}^g \\ \vdots & \ddots & \vdots \\ c_{N_{t-1},1}^p + c_{N_{t-1},1}^g & \cdots & c_{N_{t-1},N_t}^p + c_{N_{t-1},N_t}^g \end{bmatrix}, \quad (9)$$

where N_{t-1} and N_t denote the number of trajectories \mathcal{T}_{t-1} and detections \mathcal{D}_t , respectively.

Based on Eq. 9, we employ a greedy algorithm to determine associations between trajectories \mathcal{T}_{t-1} and detections \mathcal{D}_t , outputting high-quality 3D trajectories \mathcal{T}_t for frame t .

IV. EXPERIMENT

A. Dataset

We use the popular KITTI [37] and Waymo [38] tracking benchmarks to evaluate the performance of our YOOL.

TABLE I

EVALUATION RESULTS ON THE *Car* CATEGORY OF THE KITTI *test* SET. SUPERSCRIPTS \dagger AND $*$ INDICATE USING THE SAME 3D OBJECT DETECTORS, CASA [27] AND VIRCONV [28], RESPECTIVELY. NOTE THAT CASTRACK IS OPERATED IN ONLINE TRACKING MODE FOR FAIR COMPARISON. THE BEST PERFORMANCE VALUE IS IN **BOLD**.

Method	HOTA \uparrow	DetA \uparrow	AssA \uparrow	MOTA \uparrow	IDWS \downarrow	sMOTA \uparrow	FPS \uparrow
QD-3DT [29]	72.77	74.09	72.19	85.94	206	73.29	33
TripletTrack [30]	73.58	73.18	74.66	84.32	522	72.26	10
FANTrack [13]	60.85	64.36	58.69	75.84	743	61.49	25
BeyondPixels [31]	63.75	72.87	56.40	82.68	934	69.98	3
MOTSFusion [32]	68.74	72.19	66.16	84.24	415	71.14	2
PolarMOT [10]	75.16	73.94	76.95	85.08	462	71.82	50
EAFMOT [33]	72.28	71.97	73.08	84.77	107	71.56	100
NC2 [34]	71.85	69.61	64.81	78.52	159	65.46	100
mmMOT [14]	62.05	72.29	54.02	83.23	733	70.12	33
JRMOT [11]	69.61	73.05	66.89	85.10	271	72.11	14
JMODT [12]	70.73	73.45	68.76	85.35	350	72.19	22
EagerMOT [17]	74.39	75.27	74.16	87.82	239	74.97	90
DeepFusionMOT [18]	75.46	71.54	80.05	84.63	84	71.66	110
StrongFusionMOT [35]	75.65	72.08	79.84	85.53	58	72.62	100
BcMODT [36]	71.00	73.62	69.14	85.48	381	72.22	100
AB3DMOT \dagger [7]	75.72	75.64	76.45	86.93	122	74.35	210
CasTrack \dagger [9]	77.32	75.08	80.32	86.33	184	74.27	700
Ours \dagger	78.72	76.34	81.81	87.80	83	75.88	260
AB3DMOT $*$ [7]	76.53	77.98	75.82	89.01	103	76.97	210
CasTrack $*$ [9]	79.97	77.94	82.67	89.19	201	77.07	700
Ours $*$	81.02	78.94	83.83	90.31	59	78.48	260

KITTI includes 21 training sequences and 29 test sequences, with 8008 and 11095 frames, respectively. Waymo includes 798 training sequences and 202 validation sequences, each containing 20 seconds of continuous driving data. Evaluations on the *Car* and *Pedestrian* categories of KITTI, and the *Car*, *Vehicle*, and *Pedestrian* categories of Waymo, demonstrate the robustness and efficiency of our YOLOO.

B. Evaluation Metrics

We utilize the official KITTI evaluation toolkit [37], to quantitatively assess the performance of our YOLOO on KITTI. The evaluation employs CLEAR MOT metrics [39] such as Multi-Object Tracking Accuracy (MOTA), scaled MOTA (sMOTA), Multi-Object Tracking Precision (MOTP), and ID Switch (IDSW), following standard Multi-Object Tracking (MOT) rules. Additionally, the KITTI dataset incorporates the HOTA metric [40], a comprehensive MOT evaluation measure that integrates detection and association quality, further broken down into Detection Accuracy (DetA) and Association Accuracy (AssA), among others. For Waymo, MOTA is also the primary evaluation metric, considering false positives (FP), missed objects (Miss), and identity switches (IDS) at each timestamp. The evaluation performance is further categorized into two difficulty levels: LEVEL 1 and LEVEL 2. LEVEL 1 assesses objects with more than five points, whereas LEVEL 2 considers objects with at least one point. LEVEL 2 is adopted in our experiments.

C. Experimental Setup

YOLOO is developed using Python and PyTorch, with experiments conducted on a computer equipped with an Intel

Core i9 3.70GHz CPU, 64GB of RAM, and an RTX 4090 GPU. The KITTI training set is divided into two parts: a training set comprising sequences 0000, 0002, 0003, 0004, 0005, 0007, 0009, 0011, 0017, 0020, and a validation set containing sequences 0001, 0006, 0008, 0010, 0012, 0013, 0014, 0015, 0016, 0018, 0019. For Waymo, the original dataset-splitting configuration is used for training and evaluation.

During UTenc module training on KITTI and Waymo datasets, we employed an epoch count of 250, a learning rate of 0.003, and the AdamW optimizer. Image encoder input consisted of 512512 pixel patches, while the point cloud encoder processed patches containing 800 points during training and 400 points during testing. Text encoding utilized fixed-template prompts formatted as follows: “*The category of the object is category, and its location can be represented by four coordinates: (x_1 , y_1), (x_2 , y_2), (x_3 , y_3), and (x_4 , y_4).”* Here, these coordinates denote the angular positions of the object projected onto the point cloud’s X-Y plane.

Additionally, to conduct a thorough and unbiased evaluation of YOLOO, we employ a diverse set of 3D object detectors across multiple datasets. Specifically, for the KITTI dataset, we leverage Point-RCNN [41], Point-GNN [42], CasA [27], and VirConv [28]. On the Waymo dataset, we adopt the 3D detection outputs from CenterPoint [8] as the input data stream, similar to the classic SimpleTrack [19].

D. Main Results

1) *Quantitative Evaluation on KITTI*: Through comprehensive experiments on the challenging *Car* category in the KITTI test set, as shown in Table I, YOLOO demonstrates superior performance compared to 17 competing methods.

TABLE II

EVALUATION RESULTS ON THE WAYMO *validation* SET. FOR FAIRNESS, ALL COMPARED METHODS USE 3D DETECTIONS FROM CENTERPOINT AS INPUT. THE BEST PERFORMANCE VALUE IS HIGHLIGHTED IN **BOLD**, AND THE SECOND-BEST IS MARKED WITH UNDERLINED.

Method	Vehicle				Pedestrian				Cyclist				FPS \uparrow
	MOTA \uparrow	FP \downarrow	Miss \downarrow	IDS \downarrow	MOTA \uparrow	FP \downarrow	Miss \downarrow	IDS \downarrow	MOTA \uparrow	FP \downarrow	Miss \downarrow	IDS \downarrow	
AB3DMOT [7]	55.7	-	-	0.40	52.2	-	-	2.74	-	-	-	-	-
Prob3DMOT [44]	54.1	-	-	0.37	48.1	-	-	3.34	-	-	-	-	-
CenterPoint [8]	55.1	10.8	<u>33.9</u>	0.26	54.9	10.0	34.0	1.13	<u>57.4</u>	13.7	28.1	0.83	-
SimpleTrack [19]	56.1	<u>10.4</u>	33.4	<u>0.08</u>	57.8	<u>10.9</u>	<u>30.9</u>	<u>0.42</u>	56.9	<u>11.6</u>	30.9	<u>0.56</u>	2
Ours	<u>55.3</u>	10.2	34.4	0.07	<u>57.2</u>	11.6	30.8	0.40	59.5	11.1	<u>29.3</u>	0.10	80

Notably, the last six rows of Table I demonstrate that our YOLOO consistently outperforms the sophisticated CasTrack [9] and AB3DMOT [7] across all evaluation metrics when utilizing the same 3D detections from either CasA [27] or VirConv [28] as input. Specifically, when utilizing 3D detections from CasA, our method surpasses AB3DMOT by 3.00% in HOTA, 0.87% in MOTA, and 1.53% in sMOTA, while also reducing ID switches by 39. Compared to CasTrack, our method exhibits improvements of 1.40% in HOTA, 1.47% in MOTA, 1.61% in sMOTA, and a reduction of 101 ID switches. Similarly, with 3D detections from VirConv, our method yields enhancements of 4.49% in HOTA, 1.30% in MOTA, 1.51% in sMOTA, and a decrease of 44 ID switches compared to AB3DMOT. Compared to CasTrack, our method exhibits improvements of 1.05% in HOTA, 1.12% in MOTA, 1.41% in sMOTA, and a reduction of 142 ID switches. Additionally, YOLOO achieves an inference speed of over 200 FPS, comparable to AB3DMOT which employs complex Giou_3D [43] constraints, and well beyond real-time requirements (over 25 FPS). While marginally slower than CasTrack, which relies solely on center point distance and predicted scores, the substantial gains in robustness achieved by incorporating point cloud data justify this trade-off. These results collectively underscore the state-of-the-art performance of YOLOO in terms of both efficiency and robustness.

2) *Quantitative Evaluation on Waymo*: To comprehensively evaluate the generalizability of YOLOO, we conduct additional experiments on the more challenging Waymo tracking dataset. As presented in Table II, we compare our method with classic 3D MOT methods: AB3DMOT [7], Prob3DMOT [44], CenterPoint [8], and SimpleTrack [19]. For a fair comparison, all methods utilize 3D detections from CenterPoint as input. Experimental results demonstrate that our method significantly surpasses AB3DMOT, Prob3DMOT, and CenterPoint across all metrics and categories. In comparison to SimpleTrack, our method exhibits strong competitiveness, achieving an inference speed more than 40 times faster (80 FPS compared to 2 FPS), with particularly impressive results in the *Cyclist* category (59.5% MOTA vs. 56.9%). Unlike SimpleTrack, which relies on meticulously designed customized geometric constraints, fine-tuned association thresholds, and intricate tracking mechanisms, our method achieves superior performance without such complexities. Furthermore, YOLOO consistently exhibits the best performance in terms of IDS scores across all three categories. These findings underscore

the effectiveness of our method in balancing robustness and efficiency through the UTR similarity derived from UTenc and the F-GAM calculated by F-GC.

3) *Qualitative Evaluation*: To complement the quantitative analysis, qualitative evaluations are conducted on the KITTI validation set. Fig. 6 visualizes a comparison between classic AB3DMOT [7] and our YOLOO on sequence 0016, using 3D detections from Point-RCNN [41] as input. Our method demonstrates superior performance by generating more robust and accurate trajectories, effectively suppressing false trajectories, particularly those originating from erroneous detections.

E. Ablation Study

To evaluate the efficacy of UTenc and F-GC, the core components of YOLOO, we conduct ablation studies on the KITTI validation set adhering to the official KITTI evaluation protocol. Additionally, as YOLOO follows a tracking-by-detection paradigm, the quality of input 3D detections significantly influences tracking performance. To assess this impact, we also conduct experiments with different 3D detectors on the KITTI validation set.

1) *Effects of UTenc*: Under the proposed UTCL strategy, the point cloud encoder concurrently learns point cloud information alongside visual-textual knowledge derived from image and text cues during training. To assess the individual contributions of point clouds, images, and text prompts to the 3D MOT performance, Table III presents an ablation study. Results indicate that each modality enhances 3D MOT performance. When exclusively utilizing point cloud data, HOTA scores for the *Car* and *Pedestrian* categories are 71.29% and 41.28%, respectively. When integrating the image modality and text modality, respectively, the HOTA score for *Car* increased by 3.71% and 3.04%, respectively, while that for *Pedestrian* increased by 0.90% and 0.84%, respectively. The optimal performance is achieved when combining all modalities, resulting in HOTA scores of 75.84% and 44.05% for the *Car* and *Pedestrian* categories, respectively.

2) *Effects of F-GC*: From the last three rows of Table III, the effectiveness of the proposed F-GC and its advantages over the traditional C-GC are evident. Note that for C-GC, BEV_IoU with a matching threshold of 0 is employed. C-GC further improves HOTA by 0.79% and 1.07% for the *Car* and *Pedestrian* categories, respectively, while F-GC enhances HOTA by 0.79% and 2.02% for the same categories. While F-GC exhibits comparable performance to C-GC for the

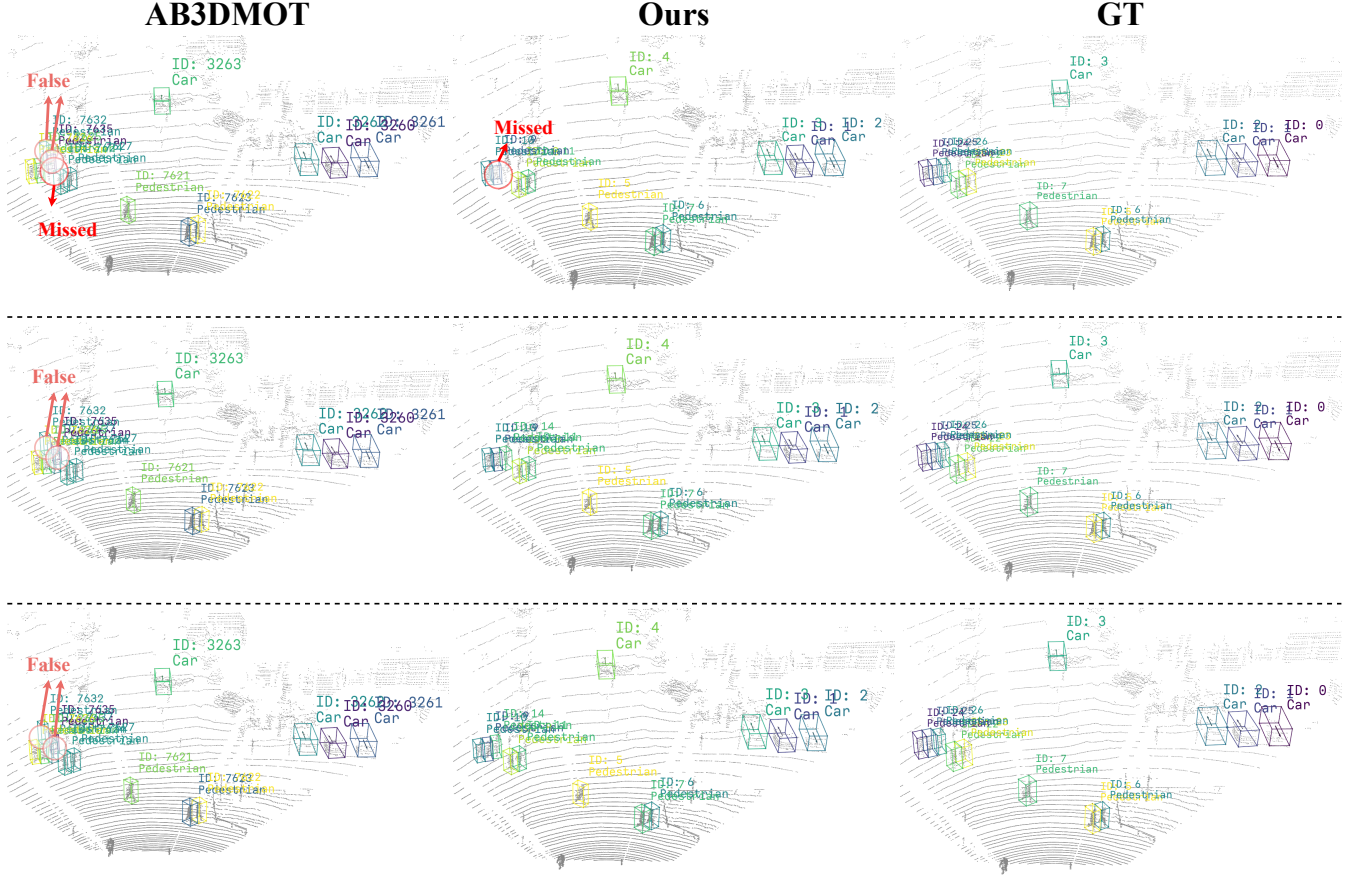


Fig. 6. **Qualitative evaluation of our YOLOO on the KITTI validation set.** This figure visualizes the tracking results on sequence *0016* using the 3D detection results of Point-RCNN as input, where each row represents a frame. Our method can generate more robust and accurate trajectories, effectively avoiding false trajectories, especially those caused by false detections.

TABLE III

ABLATION STUDY ON THE IMPACT OF DIFFERENT MODALITIES (POINT CLOUDS, IMAGES, AND TEXT CUES) AND GEOMETRIC CONSTRAINTS (GC, INCLUDING C-GC AND F-GC) ON THE 3D MOT PERFORMANCE OF OUR YOLOO, USING POINT-RCNN AS THE 3D DETECTOR FOR THE *Car* AND *Pedestrian* CATEGORIES ON THE KITTI validation set. FOR C-GC, BEV_IoU WITH A MATCHING THRESHOLD OF 0 IS EMPLOYED. THE BEST PERFORMANCE VALUE IS HIGHLIGHTED IN **BOLD**.

Modalities			GC		Car						Pedestrian					
Point Cloud	Image	Text	C-GC	F-GC	HOTA	DetA	AssA	MOTA	sMOTA	IDSW	HOTA	DetA	AssA	MOTA	sMOTA	IDSW
✓					71.29	71.74	71.10	81.41	69.64	26	41.28	42.23	40.77	52.83	29.31	190
✓	✓				75.00	72.62	77.74	82.84	71.04	26	42.18	42.61	42.20	54.84	31.47	158
✓		✓			74.33	72.64	76.37	82.73	70.95	22	42.12	42.66	42.04	54.09	30.67	166
✓	✓	✓			75.84	72.38	79.71	82.56	70.76	13	44.05	42.47	46.13	54.33	30.95	159
✓	✓	✓	✓		76.63	73.05	80.65	83.59	71.81	9	45.12	43.51	47.24	57.24	34.08	80
✓	✓	✓		✓	76.63	72.98	80.73	83.53	71.74	8	46.07	43.52	49.21	57.32	34.14	80

Car category, it demonstrates a significant advantage for the *Pedestrian* category (46.07% vs. 45.12% in HOTA). These results indicate that UTenc struggles to accurately distinguish between objects with similar appearances but distant locations, particularly for non-rigid pedestrians. Compared to C-GC, F-GC provides a more robust and complementary constraint for UTenc with more flexible and simpler computations, offering a promising foundation for future advancements.

3) *Effects of the 3D object detector*: As shown in Table IV, the choice of 3D object detectors (including PointRCNN [41], PointGNN [42], CasA [27], VirConv [28]) significantly

impacts the 3D MOT performance of YOLOO. Our results demonstrate that more advanced 3D detectors lead to better 3D MOT results. For instance, employing the state-of-the-art multi-modal 3D detector VirConv elevates YOLOO to achieve a HOTA of 85.63%, MOTA of 91.35%, and sMOTA of 83.74%, surpassing the results obtained with the earlier 3D detector Point-RCNN by a substantial margin of 9.00% in HOTA. Moreover, YOLOO consistently exhibits low IDSW across different 3D detectors, highlighting its robustness and ability to maintain stable tracking performance. This modular design of YOLOO facilitates the seamless integration of advanced 3D

TABLE IV
ABLATION STUDY ON THE IMPACT OF 3D OBJECT DETECTORS ON THE 3D MOT PERFORMANCE OF OUR YOLOO FOR THE *Car* CATEGORY ON THE KITTI validation SET. THE BEST PERFORMANCE VALUE IS HIGHLIGHTED IN **BOLD**.

3D Object Detector				HOTA	DetA	AssA	MOTA	sMOTA	IDSW
Point-RCNN	Point-GNN	CasA	VirConv						
✓				76.63	72.98	80.73	83.53	71.74	8
	✓			79.78	78.49	81.33	89.35	78.03	8
		✓		83.42	81.39	85.65	89.87	80.73	4
			✓	85.63	84.84	86.52	91.35	83.74	8

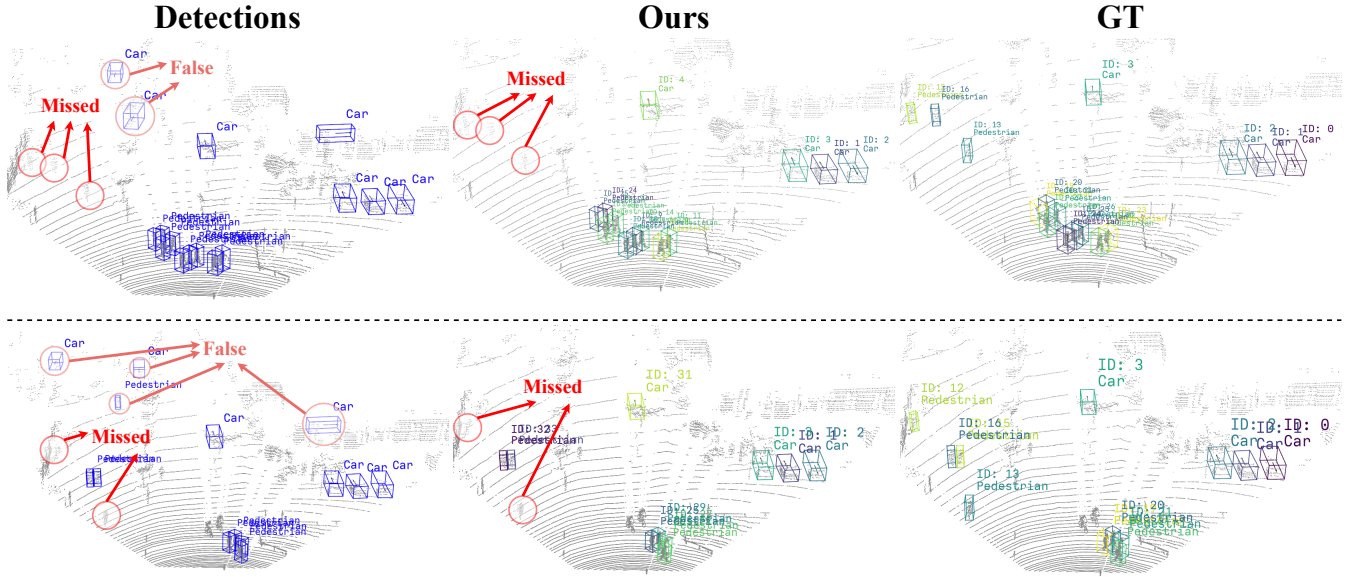


Fig. 7. **Failures of our YOLOO on the KITTI validation set.** It illustrates the tracking results on the sequence *0016*, using 3D detection results of Point-RCNN as input, where each row represents a frame. While our method effectively mitigates false detections and maintains tracking stability, it exhibits limitations in addressing missed detections, which can hinder its overall performance.

detectors, promising continuous performance improvements.

V. LIMITATIONS

YOLOO exhibits several limitations. Firstly, while YOLOO is robust in processing input 3D detections, it remains susceptible to the limitations of the underlying 3D detector. As illustrated in Fig. 7, missed detections in the input data directly impact the accuracy of the output trajectories. Secondly, while UTenc effectively learns robust unified representations from diverse modalities, it remains susceptible to confusion between visually similar objects in different spatial locations, necessitating the auxiliary constraints of F-GC. Thirdly, the point cloud encoder within UTenc excels in handling dense point clouds as found in datasets like KITTI and Waymo collected using 64-beam LiDARs. However, it struggles with sparse point clouds. For instance, the nuScenes dataset [45] collected with a 32-beam LiDAR often provides sparse point cloud representations, especially for distant objects, which can be represented by only one or two points (see Fig. 8). In light of these limitations, our ongoing efforts are dedicated to developing efficient and robust multi-modal 3D MOT solutions.

VI. CONCLUSION

We introduce YOLOO, a novel multi-modal 3D object tracking (MOT) solution that redefines the conventional multi-modal paradigm. YOLOO harnesses multi-modal information (including point clouds, images, and even text cues) during training to learn robust representations. Uniquely, YOLOO performs inference exclusively on point cloud data, resulting in substantial computational efficiency gains compared to traditional multi-modal methods. Specifically, YOLOO includes two core components: a unified tri-modal encoder (UTenc) and a flexible geometric constraint (F-GC) module. UTenc fuses rich visual-language representations from pre-trained visual-language models (VLMs, e.g., CLIP) into the point cloud encoder through a proposed unified tri-modal contrastive learning scheme. This innovation allows for inference using only the point cloud encoder to generate a unified tri-modal representation (UTR) for object similarity discrimination. Additionally, F-GC calculates a flexible geometric alignment metric (F-GAM) to discriminate objects with significant geometric positional differences, without the need for scene-specific fine-tuning. Leveraging the UTR similarity and the F-GAM, YOLOO accurately associates trajectories and detec-

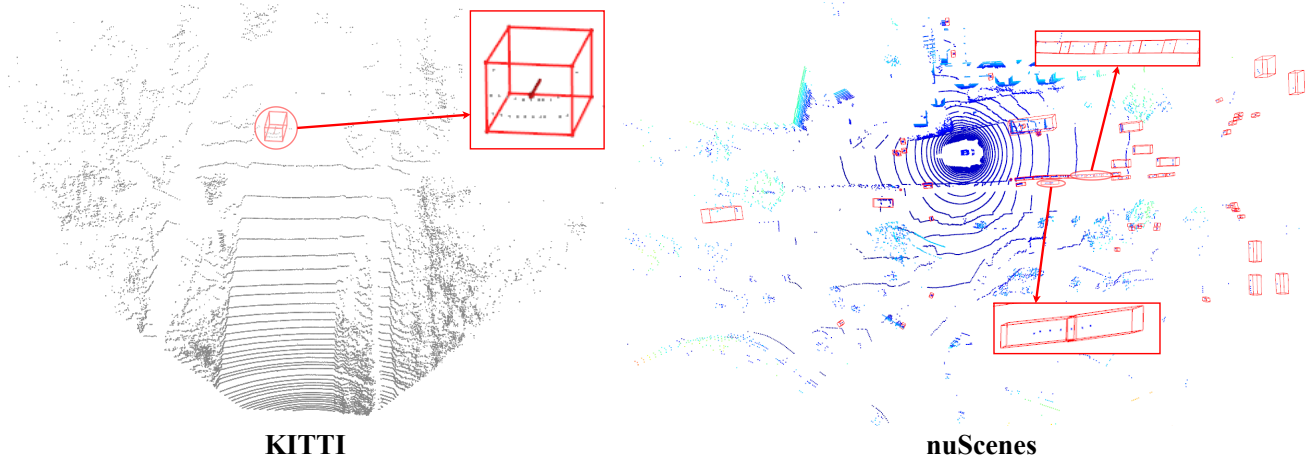


Fig. 8. **Visualization of point cloud samples from KITTI and nuScenes.** The left side shows point clouds from the KITTI dataset collected with a 64-beam LiDAR, which are dense, even for distant objects. In contrast, the right side shows point clouds from the nuScenes dataset collected with a 32-beam LiDAR, which are sparse, with only a very limited number of points on slightly distant objects.

tions across frames, producing high-quality 3D trajectories.

Our work demonstrates the transformative potential of pre-trained VLMs and textual information in advancing multi-modal 3D MOT research, paving the way for an efficient and robust solution. We anticipate that YOLOO will inspire future research and development in the field of multi-modal 3D MOT.

REFERENCES

- [1] A. Bewley, Z. Ge, L. Ott, F. T. Ramos, and B. Upcroft, “Simple online and realtime tracking,” in *IEEE International Conference on Image Processing*, 2016, pp. 3464–3468.
- [2] N. Wojke, A. Bewley, and D. Paulus, “Simple online and realtime tracking with a deep association metric,” in *IEEE International Conference on Image Processing*, 2017, pp. 3645–3649.
- [3] F. Zeng, B. Dong, Y. Zhang, T. Wang, X. Zhang, and Y. Wei, “MOTR: end-to-end multiple-object tracking with transformer,” in *Computer Vision - ECCV 2022 - 17th European Conference*, ser. Lecture Notes in Computer Science, S. Avidan, G. J. Brostow, M. Cissé, G. M. Farinella, and T. Hassner, Eds., vol. 13687, 2022, pp. 659–675.
- [4] Y. Zhang, T. Wang, and X. Zhang, “Motrv2: Bootstrapping end-to-end multi-object tracking by pretrained object detectors,” *CoRR*, vol. abs/2211.09791, 2022.
- [5] Y. Du, Y. Song, B. Yang, and Y. Zhao, “Strongsort: Make deepsort great again,” *CoRR*, vol. abs/2202.13514, 2022.
- [6] Z. Zhao, Z. Wu, Y. Zhuang, B. Li, and J. Jia, “Tracking objects as pixel-wise distributions,” in *Computer Vision - ECCV 2022 - 17th European Conference, Proceedings, Part XXII*, ser. Lecture Notes in Computer Science, S. Avidan, G. J. Brostow, M. Cissé, G. M. Farinella, and T. Hassner, Eds., vol. 13682, 2022, pp. 76–94.
- [7] X. Weng, J. Wang, D. Held, and K. Kitani, “AB3DMOT: A baseline for 3d multi-object tracking and new evaluation metrics,” *CoRR*, vol. abs/2008.08063, 2020.
- [8] T. Yin, X. Zhou, and P. Krähenbühl, “Center-based 3d object detection and tracking,” in *IEEE Conference on Computer Vision and Pattern Recognition*, 2021, pp. 11 784–11 793.
- [9] H. Wu, W. Han, C. Wen, X. Li, and C. Wang, “3d multi-object tracking in point clouds based on prediction confidence-guided data association,” *IEEE Trans. Intell. Transp. Syst.*, vol. 23, no. 6, pp. 5668–5677, 2022.
- [10] A. Kim, G. Brasó, A. Osep, and L. Leal-Taixé, “Polarmot: How far can geometric relations take us in 3d multi-object tracking?” in *Computer Vision - ECCV 2022 - 17th European Conference, Proceedings, Part XXII*, S. Avidan, G. J. Brostow, M. Cissé, G. M. Farinella, and T. Hassner, Eds., vol. 13682, 2022, pp. 41–58.
- [11] A. Sheno, M. Patel, J. Gwak, P. Goebel, A. Sadeghian, H. Rezatofighi, R. Martín-Martín, and S. Savarese, “JRMOT: A real-time 3d multi-object tracker and a new large-scale dataset,” in *IEEE/RSJ International Conference on Intelligent Robots and Systems*, 2020, pp. 10 335–10 342.
- [12] K. Huang and Q. Hao, “Joint multi-object detection and tracking with camera-lidar fusion for autonomous driving,” in *IEEE/RSJ International Conference on Intelligent Robots and Systems*, 2021, pp. 6983–6989.
- [13] E. Baser, V. Balasubramanian, P. Bhattacharyya, and K. Czarnecki, “Fantrack: 3d multi-object tracking with feature association network,” in *IEEE Intelligent Vehicles Symposium*, 2019, pp. 1426–1433.
- [14] W. Zhang, H. Zhou, S. Sun, Z. Wang, J. Shi, and C. C. Loy, “Robust multi-modality multi-object tracking,” in *IEEE/CVF International Conference on Computer Vision*, 2019, pp. 2365–2374.
- [15] A. Radford, J. W. Kim, C. Hallacy, A. Ramesh, G. Goh, S. Agarwal, G. Sastry, A. Askell, P. Mishkin, J. Clark *et al.*, “Learning transferable visual models from natural language supervision,” in *International conference on machine learning*, 2021, pp. 8748–8763.
- [16] R. Girdhar, A. El-Nouby, Z. Liu, M. Singh, K. V. Alwala, A. Joulin, and I. Misra, “Imagebind one embedding space to bind them all,” in *IEEE/CVF Conference on Computer Vision and Pattern Recognition*, 2023, pp. 15 180–15 190.
- [17] A. Kim, A. Osep, and L. Leal-Taixé, “Eagermot: 3d multi-object tracking via sensor fusion,” in *IEEE International Conference on Robotics and Automation, ICRA 2021, Xi’an, China, May 30 - June 5, 2021*, 2021, pp. 11 315–11 321.
- [18] X. Wang, C. Fu, Z. Li, Y. Lai, and J. He, “Deepfusionmot: A 3d multi-object tracking framework based on camera-lidar fusion with deep association,” *IEEE Robotics Autom. Lett.*, vol. 7, no. 3, pp. 8260–8267, 2022.
- [19] Z. Pang, Z. Li, and N. Wang, “Simpletrack: Understanding and rethinking 3d multi-object tracking,” in *Computer Vision - ECCV 2022 Workshops*, vol. 13801, 2022, pp. 680–696.
- [20] Z. Liu, T. Huang, B. Li, X. Chen, X. Wang, and X. Bai, “Epnet++: Cascade bi-directional fusion for multi-modal 3d object detection,” *IEEE Trans. Pattern Anal. Mach. Intell.*, vol. 45, no. 7, pp. 8324–8341, 2023.
- [21] L. Gu, X. Yan, P. Cui, L. Gong, H. Xie, F. L. Wang, J. Qin, and M. Wei, “Pointsee: Image enhances point cloud,” *CoRR*, vol. abs/2211.01664, 2022.
- [22] W. Kuo, Y. Cui, X. Gu, A. Piergiovanni, and A. Angelova, “F-vlm: Open-vocabulary open-vocabulary object detection upon frozen vision and language models,” *arXiv preprint arXiv:2209.15639*, 2022.
- [23] Y. Du, F. Wei, Z. Zhang, M. Shi, Y. Gao, and G. Li, “Learning to prompt for open-vocabulary object detection with vision-language model,” in *IEEE/CVF Conference on Computer Vision and Pattern Recognition*, 2022, pp. 14 064–14 073.
- [24] S. Wu, W. Zhang, S. Jin, W. Liu, and C. C. Loy, “Aligning bag of regions for open-vocabulary object detection,” in *IEEE/CVF Conference on Computer Vision and Pattern Recognition*, 2023, pp. 15 254–15 264.
- [25] C. R. Qi, L. Yi, H. Su, and L. J. Guibas, “Pointnet++: Deep hierarchical feature learning on point sets in a metric space,” in *Advances in Neural Information Processing Systems 30: Annual Conference on Neural Information Processing Systems*, 2017, pp. 5099–5108.
- [26] H. Zhao, L. Jiang, J. Jia, P. H. Torr, and V. Koltun, “Point transformer,”

- in *IEEE/CVF international conference on computer vision*, 2021, pp. 16 259–16 268.
- [27] H. Wu, J. Deng, C. Wen, X. Li, C. Wang, and J. Li, “Casa: A cascade attention network for 3-d object detection from lidar point clouds,” *IEEE Trans. Geosci. Remote. Sens.*, vol. 60, pp. 1–11, 2022.
 - [28] H. Wu, C. Wen, S. Shi, X. Li, and C. Wang, “Virtual sparse convolution for multimodal 3d object detection,” in *IEEE/CVF Conference on Computer Vision and Pattern Recognition*, 2023, pp. 21 653–21 662.
 - [29] H.-N. Hu, Y.-H. Yang, T. Fischer, T. Darrell, F. Yu, and M. Sun, “Monocular quasi-dense 3d object tracking,” *IEEE Transactions on Pattern Analysis and Machine Intelligence*, vol. 45, no. 2, pp. 1992–2008, 2022.
 - [30] N. Marinello, M. Proesmans, and L. V. Gool, “Triplettrack: 3d object tracking using triplet embeddings and LSTM,” in *IEEE/CVF Conference on Computer Vision and Pattern Recognition Workshops*, 2022, pp. 4499–4509.
 - [31] S. Sharma, J. A. Ansari, J. K. Murthy, and K. M. Krishna, “Beyond pixels: Leveraging geometry and shape cues for online multi-object tracking,” in *IEEE International Conference on Robotics and Automation*, 2018, pp. 3508–3515.
 - [32] J. Luiten, T. Fischer, and B. Leibe, “Track to reconstruct and reconstruct to track,” *IEEE Robotics Autom. Lett.*, vol. 5, no. 2, pp. 1803–1810, 2020.
 - [33] J. Jin, J. Zhang, K. Zhang, Y. Wang, Y. Ma, and D. Pan, “3d multi-object tracking with boosting data association and improved trajectory management mechanism,” *Signal Process.*, vol. 218, p. 109367, 2024.
 - [34] C. Jiang, Z. Wang, H. Liang, and Y. Wang, “A novel adaptive noise covariance matrix estimation and filtering method: Application to multi-object tracking,” *IEEE Trans. Intell. Veh.*, vol. 9, no. 1, pp. 626–641, 2024.
 - [35] X. Wang, C. Fu, J. He, S. Wang, and J. Wang, “Strongfusionmot: A multi-object tracking method based on lidar-camera fusion,” *IEEE Sensors Journal*, 2022.
 - [36] K. Zhang, Y. Liu, F. Mei, J. Jin, and Y. Wang, “Boost correlation features with 3d-miou-based camera-lidar fusion for modt in autonomous driving,” *Remote Sensing*, vol. 15, no. 4, p. 874, 2023.
 - [37] A. Geiger, P. Lenz, and R. Urtasun, “Are we ready for autonomous driving? the KITTI vision benchmark suite,” in *IEEE Conference on Computer Vision and Pattern Recognition*, 2012, pp. 3354–3361.
 - [38] P. Sun, H. Kretzschmar, X. Dotiwalla, A. Chouard, V. Patnaik, P. Tsui, J. Guo, Y. Zhou, Y. Chai, B. Caine, V. Vasudevan, W. Han, J. Ngiam, H. Zhao, A. Timofeev, S. Ettinger, M. Krivokon, A. Gao, A. Joshi, Y. Zhang, J. Shlens, Z. Chen, and D. Anguelov, “Scalability in perception for autonomous driving: Waymo open dataset,” in *IEEE/CVF Conference on Computer Vision and Pattern Recognition*, 2020, pp. 2443–2451.
 - [39] K. Bernardin and R. Stiefelhagen, “Evaluating multiple object tracking performance: The CLEAR MOT metrics,” *EURASIP J. Image Video Process.*, vol. 2008, 2008.
 - [40] J. Luiten, A. Osep, P. Dendorfer, P. H. S. Torr, A. Geiger, L. Leal-Taixé, and B. Leibe, “HOTA: A higher order metric for evaluating multi-object tracking,” *Int. J. Comput. Vis.*, vol. 129, no. 2, pp. 548–578, 2021.
 - [41] S. Shi, X. Wang, and H. Li, “Pointcnn: 3d object proposal generation and detection from point cloud,” in *IEEE Conference on Computer Vision and Pattern Recognition*, 2019, pp. 770–779.
 - [42] W. Shi and R. Rajkumar, “Point-gnn: Graph neural network for 3d object detection in a point cloud,” in *IEEE/CVF Conference on Computer Vision and Pattern Recognition*, 2020, pp. 1708–1716.
 - [43] J. Xu, Y. Ma, S. He, and J. Zhu, “3d-giou: 3d generalized intersection over union for object detection in point cloud,” *Sensors*, vol. 19, no. 19, p. 4093, 2019.
 - [44] H.-k. Chiu, A. Prioletti, J. Li, and J. Bohg, “Probabilistic 3d multi-object tracking for autonomous driving,” *arXiv preprint arXiv:2001.05673*, 2020.
 - [45] H. Caesar, V. Bankiti, A. H. Lang, S. Vora, V. E. Liong, Q. Xu, A. Krishnan, Y. Pan, G. Baldan, and O. Beijbom, “nusenes: A multimodal dataset for autonomous driving,” in *IEEE Conference on Computer Vision and Pattern Recognition*, 2020, pp. 11 618–11 628.